Marine Geology, 60 (1984) 165—198
Elsevier Science Publishers B.V., Amsterdam — Printed in The Netherlands

WAVE-FORMED STRUCTURES AND PALEOENVIRONMENTAL RECONSTRUCTION

H. EDWARD CLIFTON and JOHN R. DINGLER

U.S. Geological Survey, 345 Middlefield Road, Menlo Park, CA 94025 (U.S.A.)

(Received September 15, 1983; revised and accepted January 14, 1984)

ABSTRACT

Clifton, H.E. and Dingler, J.R., 1984. Wave-formed structures and paleoenvironmental reconstruction. In: B. Greenwood and R.A. Davis, Jr. (Editors), Hydrodynamics and Sedimentation in Wave-Dominated Coastal Environments. Mar. Geol., 60: 165—198.

Wave-formed sedimentary structures can be powerful interpretive tools because they reflect not only the velocity and direction of the oscillatory currents, but also the length of the horizontal component of orbital motion and the presence of velocity asymmetry within the flow. Several of these aspects can be related through standard wave theories to combinations of wave dimensions and water depth that have definable natural limits. For a particular grain size, threshold of particle movement and that of conversion from a rippled to flat bed indicate flow-velocity limits. The ratio of ripple spacing to grain size provides an estimate of the length of the near-bottom orbital motion. The degree of velocity asymmetry is related to the asymmetry of the bedforms, though it presently cannot be estimated with confidence. A plot of water depth versus wave height (h—H diagram) provides a convenient approach for showing the combination of wave parameters and water depths capable of generating any particular structure in sand of a given grain size. Natural limits on wave height and inferences or assumptions regarding either water depth or wave period based on geologic evidence allow refinement of the paleoenvironmental reconstruction. The assumptions and the degree of approximation involved in the different techniques impose significant constraints. Inferences based on wave-formed structures are most reliable when they are drawn in the context of other evidence such as the association of sedimentary features or progradational sequences.

INTRODUCTION

Sedimentary geologists have long sought to use depositional structures for interpreting ancient depositional environments. Quantitative analysis of paleo-processes based on such structures has proved at best only partly successful. Even where the structures can be related with reasonable precision to ancient processes, those processes commonly cannot be meaningfully incorporated into a broader environmental interpretation. For example, the flow-regime concept provides a comprehensive model for interpreting structures produced by unidirectional flow (Harms et al., 1982). Nonetheless, even where application of the concept generates specific data on such parameters as flow velocity and water depth, it commonly is unclear how these parameters contribute significantly to a paleoenvironmental reconstruction.

0025-3227/84/$03.00

In contrast, parameters interpreted from wave-generated structures commonly can be linked clearly to important aspects of the depositional setting. Water depth, for example, which is of somewhat uncertain influence on the development of structures produced by unidirectional flow, bears in a direct, calculable way on the origin and nature of wave-formed structures.

Until recently, wave-generated sedimentary structures were poorly understood, and, consequently, they could not be used to successfully interpret depositional environments. Considerable data based on field and laboratory experiments and observations have accumulated in recent years (for example, Lofquist, 1978; Miller and Komar, 1980a, b; Dingler and Clifton, 1984, this volume), and several interpretative models have been proposed based on wave-generated structures (e.g., Allen, 1970; Tanner, 1971; Komar, 1974; Clifton, 1976; Allen, 1979, 1980, 1982; Harms et al., 1982). Although the relations between wave-generated structures and the associated fluid dynamics are still not fully understood, useful interpretations are possible. This paper summarizes the published research on wave-formed sedimentary structures and outlines a procedure whereby wave-formed structures can be used to interpret ancient depositional environments. The procedure is presented step by step, noting the physical basis for the parameters employed, and assessing the validity of the various approaches and techniques. In conclusion the procedure is applied to specific geological problems.

THE INTERPRETIVE PROCEDURE

The procedure of interpreting paleoenvironments from wave-generated structures requires three discrete steps. The first involves inferring flow parameters from specific aspects of the wave-generated structures using results from empirical investigations or experimental studies. The second step employs wave theory to determine the combinations of water depth and wave size and shape that could produce the inferred flow parameters. The third step utilizes the natural limits that exist for waves, geologic reasoning, or wave-hindcasting techniques to constrain the range of possible combinations of water depth and wave size and to relate those that are feasible to the paleoenvironment.

STEP 1. INFERRING FLOW PARAMETERS FROM WAVE-FORMED FEATURES

Wave-formed structures

Under wave action, the character of the flow and the composition of the bed (texture and mineralogy) combine to determine the general configuration of the bed (flat, hummocky, or rippled) and the size and shape of the bedforms themselves. Accordingly, aspects of size and shape of the bedforms can be used to infer previously existing flow parameters, which can in turn be applied to the interpretation of depositional environments.

Oscillation ripples are the predominant wave-generated bedforms. In profile, spacing λ, height η and symmetry β/λ characterize these ripples (Fig. 1). In

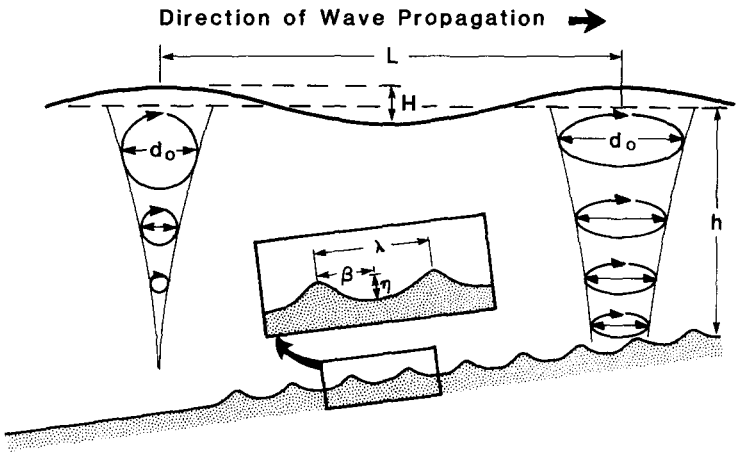

Fig.1. Geologically important parameters of waves, water motion and wave-formed ripples. Wave length (L) is the horizontal distance between successive wave crests; wave height (H) is the vertical distance between wave crest and trough; water depth (h) is the vertical distance from still water level to the seafloor; orbital diameter (d_0) is the maximum horizontal distance of excursion of water particles as a wave passes (a circular motion in deep water, an elliptical motion in shallow water); ripple spacing (λ) is the average horizontal distance between ripple crests; ripple height (η) is the average vertical distance between ripple crests and troughs; ripple asymmetry (β/λ) is the ratio between the average distance from ripple crest to leading trough (β) and the average ripple spacing (λ). Not shown: the wave period (T), the time required for successive wave crests to pass a given point; and the maximum orbital velocity (u_m), the maximum horizontal velocity in the direction of wave passage.

plan, crest length relative to spacing and crest sinuosity are primary characteristics; Inman (1957) called ripples short-crested, intermediate-crested, or long-crested if their crest-length to spacing ratio was less than 3, 3—8, or greater than 8, respectively. Crest pattern ranges from straight to sinuous; in the extreme they can take on a crescentic shape, such as the lunate megaripples of Clifton et al. (1971). Most oscillation ripples are transverse to the forming current, but a few types such as the cross ripples described by Clifton et al. (1971) are oblique to the flow.

The ratio of ripple height to wavelength η/λ is the ripple steepness; it and its inverse, the ripple index (Reineck and Singh, 1973) or vertical form index (Bucher, 1919), have been used to describe ripples (e.g., Dingler, 1974; Allen, 1980). Allen (1980) indicates that a wide range of ripple indices (steepnesses) is possible. Dingler and Inman (1977) showed that for fine sand near La Jolla, California, ripple steepness remained at a value of about 0.15 with increasing wave energy until, as sheet flow conditions were approached, the steepness decreased systematically to zero.

Symmetric ripples have a symmetry factor (β/λ) that approaches 0.5, or a ripple symmetry index [$(\lambda - \beta)/\beta$; Reineck and Singh, 1973] that approaches 1.0. The steeper side of most asymmetric ripples faces in the direction of ripple migration, making the symmetry factor less than 0.5 and the ripple

symmetry index greater than 1.0. The maximum value of the ripple symmetry index acquired by asymmetric wave ripples is reportedly 3.8 (Reineck and Singh, 1973, p.27), equivalent to a symmetry factor of about 0.25.

The nature of the sediment that composes the bed is an important and potentially troublesome factor. Several different aspects of texture or composition such as mean grain size (D), sorting, shape, and particle density can bear on bedform development. The influence of mean grain size is fairly well known (Clifton, 1976), but very little is known about the effects of the other three factors. It would seem likely, however, that a bed of coquina would respond to a given type of flow differently than would a bed of quartz sand of similar mean grain size.

The recognition of structures as formed by waves is obviously critical to their use as interpretive tools. Symmetric ripples are generally accepted a priori as produced by wave activity, although the common presence of symmetrical ripples in deep-sea photographs (Heezen and Hollister, 1971, p.348) suggests other possible mechanisms. Asymmetric bedforms generated by waves may be difficult to distinguish from those formed by unidirectional currents. Tanner (1967), Reineck and Wunderlich (1968), Boersma (1970), and Reineck and Singh (1973) present criteria for recognizing wave-produced bedforms.

The problem of identifying effects of waves is further complicated in exposures where the bedforms themselves are poorly expressed. In such a case, the influence of waves must be inferred, often with difficulty, from the internal structure produced by migrating bedforms. Boersma (1970) and Allen (1982) offer a number of criteria for recognizing wave-formed ripples on the basis of internal structure. The orientation of the ripples can in some cases suggest their origin. Because of the general absence of shoreward-flowing currents, Clifton (1981) inferred that ripples that faced or migrated in a shoreward direction were solely the product of waves.

Most of the expressed relationships between wave-formed structures, flow parameters, and waves assume an absence of superimposed unidirectional current (Clifton, 1976; Allen, 1981a). Yet in natural environments, combined oscillatory and unidirectional flow, in the form of tidal, rip or longshore currents is fairly common. A few studies have described combined flow ripples (Reineck and Wunderlich, 1968; Harms, 1969; Bliven et al., 1977), but presently they cannot be used with confidence in environmental interpretation (Harms et al., 1982, pp.2—42). Distinguishing between purely oscillatory and combined-flow ripples may be very difficult.

The identification of flat bedding produced by oscillatory sheet flow can be particularly difficult. First, it may be impossible to recognize the contribution of superimposed unidirectional flow to the development of sheet flow conditions. Second, ripples that migrate across the seafloor may produce a very similar, nearly flat stratification that is analogous to the climbing translatent strata observed in eolian deposits (Hunter, 1977). Clifton (1976) suggests several criteria (mostly based on lithologic association) that may prove useful for distinguishing between sheet-flow laminae and subaqueous climbing translatent strata.

Flow parameters

The flow parameters that can be inferred from wave-generated structures are relatively straightforward. As a wave travels along the surface of the water, it sets the water particles in motion (Fig.1). If the water depth (h) is large relative to the length (L) of wave (that is, $h > L/4$), the wave form is sinusoidal and the induced water motion is essentially circular (Fig.1). The diameter of the circle (d_0) diminishes exponentially with depth, reaching zero above the bottom. In shallower water, where the wave interacts with the bottom, the wave may retain its nearly sinusoidal shape, but the water particles move in ellipses that become progressively flatter and smaller with depth (Fig.1). Just above the sea floor the elliptical motion becomes a horizontal oscillation, the length of which still is referred to as "orbital diameter". In very shallow water, just before breaking, the wave may lose its sinusoidal shape, and the water motion is nearly horizontal throughout the water column (Komar, 1976).

The velocity of the water particles, which is a critical parameter in the threshold of grain movement and in the shaping of bedforms, depends both on the magnitude of the orbital diameter and on the wave period (T). For deep-water waves (where water motion is circular), the maximum orbital velocity (u_m) equals the average orbital velocity, the circumference of the orbital motion (πd_0) divided by the time required to complete an orbit (T). In shallower water, the maximum orbital velocity above the bottom differs from the average velocity, but the relation, $u_m = \pi d_0/T$, remains valid.

As a wave approaches the shore, its form changes (Fig.2) such that the crest becomes increasingly narrow and peaked and the trough broad and flat. As the wave begins to break, it also becomes asymmetric about a vertical plane through and parallel to the crest, because its landward face steepens relative to its seaward face. These changes impart an asymmetry to the orbital motion.

Part of the physical basis for this asymmetry can be seen in Fig.2. If mass transport is assumed to be nil, the volume of water that moves forward under the crest of a wave must equal that which moves in the opposite direction under the trough. Because the crest of the wave is foreshortened relative to

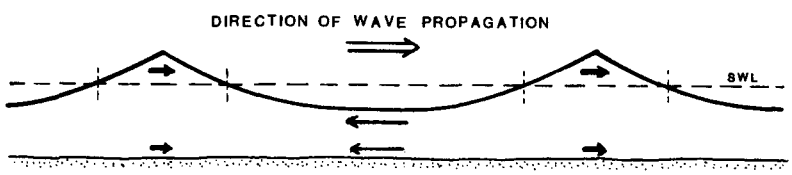

Fig.2. Typical form of a wave as it passes into shallow water. Note that the time available for movement of water in the direction of wave propagation under the crest of the wave is substantially less than that available for movement in the opposite direction under the wave trough. The result is a velocity—magnitude and velocity—time asymmetry whereby the forward motion of the water under the crest is strong but of short duration relative to the reverse motion under the trough.

the trough, water under the crest must move more rapidly to maintain mass balance. This condition causes the bottom orbital flow under the crest to be abrupt and strong relative to that under the trough. This onshore flow would be further reinforced by any shoreward mass transport.

The resulting orbital velocity asymmetry can be viewed as consisting of both a velocity-magnitude and a velocity—time component (Kemp, 1975). Velocity—magnitude asymmetry, as used here, refers to any difference between the peak or maximum velocity under the crest and trough of the wave. Velocity—time asymmetry refers to any difference between the duration of flow in the direction of wave propagation and that in the opposite direction. Figure 3 illustrates some of the conceivable velocity profiles that could be generated by shoaling waves. It should be noted that, in nature, asymmetry of flow is almost always due to a combination of velocity—magnitude and velocity—time asymmetry and is therefore complex.

The amount of water mass transport generated by asymmetric orbital motions seems variable and, under certain conditions, may be of minimal importance. The character of flow was qualitatively examined over a field of shoreward-facing lunate megaripples located seaward of the surf zone on the southern Oregon coast, using neutrally buoyant drifters, vertical streaks of dye, and clouds of sand thrown into suspension on the leeward side of the lunate megaripples (Clifton et al., 1971). In no case evidence was seen for shoreward water mass transport, even as the lunate megaripples migrated towards the shore.

In summary, orbital velocity asymmetry derives from differences in magnitude and duration of the back-and-forth components of oscillatory flow. Both aspects are important to the movement of sediment. Velocity-magnitude asymmetry is particularly important where only the stronger component exceeds the threshold velocity for movement of a given grain size (Kemp, 1975). Moreover, since bedload transport is thought to vary approximately with the third or fourth power of velocity (Inman, 1963; Wells, 1967), velocity—magnitude asymmetry may significantly influence onshore/offshore sediment transport. Net water transport is an additional factor that may be most important for the movement of suspended fine sand (Kemp, 1975).

Because of the complexities involved, an acceptable measure of velocity asymmetry is yet to be defined. Clifton's (1976) parameter Δu_m is the absolute difference in the peak orbital velocity under the crest and the trough of a wave; Kemp's parameter ν_m is the ratio between the two. Neither measure takes into account the duration of the opposing flows which must be accounted as important. Other authors (Dingler, 1974; Allen, 1979, 1980) measure orbital asymmetry in terms of the associated net drift of the water or the ratio of this drift to maximum orbital velocity. This approach does not accommodate the important influence of the velocity—magnitude asymmetry. Kemp (1975) suggests using the time—velocity curves to estimate the potential transport of a grain of a particular size. Such a process is laborious but should give the most reliable measure of the effects of orbital velocity asymmetry.

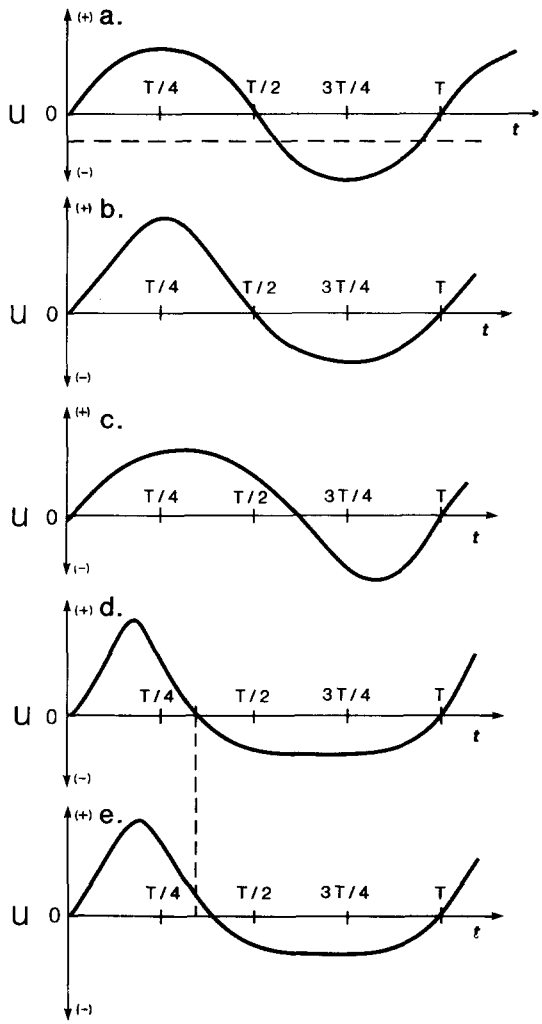

Fig.3. Possible profiles of velocity (u) over time (t) imparted by a wave of period T. Vertical axis = velocity (positive in the direction of wave approach); horizontal axis = time. (a) Neither velocity—magnitude nor velocity—time asymmetry; no net transport (typical symmetrical velocity profile under a sinusoidal wave; common in nature). (b) Velocity—magnitude asymmetry without velocity—time asymmetry; probable net transport in direction of stronger flow (not likely to occur in nature). (c) Velocity—time asymmetry without velocity—magnitude asymmetry; probable net flow in the direction of flow with longer duration (not likely to occur in nature). (d) Both velocity—magnitude and velocity—time asymmetry, balanced such that net transport is negligible (observed qualitatively over active highly asymmetric bedforms just seaward from the southern Oregon surf zone). (e) Both velocity—magnitude and velocity—time asymmetry, some net transport in direction of wave propagation. Note subtle difference from profile d (may be common under natural shoaling waves). Note that a superimposed unidirectional flow can impart both velocity—magnitude and velocity—time asymmetry to any of the profiles including profile a, where the effect can be visualized by adding a constant velocity to the curve shown (i.e., moving the curve up or down relative to the zero-velocity axis.

The velocity asymmetry induced by shoaling waves is extremely important in the sorting and transport of sand and in the development of sedimentary structures. It is, however, complex, involving both differences in the velocity components of oscillatory currents and a net transport of water. The issue can be further complicated by the presence of unidirectional flows such as rip currents or wind-driven flow, that are unrelated to the currents induced by the passing wave, but can further modify their character (e.g., Inman and Bowen, 1963).

Basis for inference of flow parameters

The basis for inferring the foregoing flow parameters from wave-generated structures lies largely in either empirical analysis of field data or experimental studies in the laboratory. Neither of these approaches produces completely satisfactory results relative to geological applications. Field studies encompass such a large number of variables that it is difficult to ascertain the critical relationships, and the spectre of metastability haunts the results. Laboratory experiments can reduce the number of variables and can generate equilibrium conditions; commonly, however, such experiments cannot satisfactorily duplicate natural conditions.

One approach to dealing with the variables encountered in field studies is to make simplifying assumptions regarding the viscosity and density of the water and the size, shape, and density of the sediment (Clifton, 1976). Some of these assumptions, unfortunately, have little basis. Although wave-winnowed sand typically is well-sorted, it is not uniform in texture and composition.

Metastability can be an important problem attending empirical studies in that the observed bedforms may not be completely in equilibrium with the processes active at the time of observation (Harms et al., 1982). Disequilibrium may result from two different factors. First, the observed bedforms may have developed under more energetic conditions than those at the time of observation and retained their initial form under the influence of less intense processes. Second, the bedforms themselves may influence the flow in such a way as to retain their original character. Commonly it is impossible to establish in the field if the observed structures are responding completely to ongoing processes without prior influence.

Laboratory studies circumvent many of these problems because sand of uniform size can be used as bed material and the waves, or flow, carefully controlled. Although these experimental studies can do much to define the influence of specific flow parameters, they can duplicate only a small range of natural environmental conditions. Specifically, laboratory studies have yet to replicate conditions imposed by large, long-period oceanic waves. Moreover, certain types of experimental techniques (specifically the use of an oscillating bed) may produce misleading results (Miller and Komar, 1980a; Harms et al., 1982).

Empirical and experimental studies of wave-generated bedforms provide the basis for interpreting maximum orbital velocity, orbital diameter, wave

period, and questionably, orbital velocity asymmetry. Estimates of orbital velocity are based on threshold criteria for grain movement or for sheet flow. Estimates of orbital diameter are predicated on the relation of ripple spacing or steepness to grain size. Estimates of orbital velocity asymmetry derive from the degree of asymmetry of the depositional structures.

Threshold velocities

Two threshold velocities can be defined for oscillatory flow: that required to initiate grain movement and that required to produce sheet flow. Under the oscillatory currents produced by surface gravity waves, ripples form quickly upon the initiation of grain movement (Dingler, 1974); the lower flat-bed regime that occurs in unidirectional flow appears to be largely suppressed. Bagnold (1946), Komar and Miller (1973, 1975), and Dingler (1979) are among several investigators who have studied the threshold of grain motion in oscillatory flow. The relation for the onset of grain motion under oscillatory flow resembles the Shields (1936)—Bagnold (1966) relationship for onset under unidirectional flow (Madsen and Grant, 1976; Dingler, 1979).

Threshold criteria are most accurately presented in terms of shear stress, τ, which is related to the mean velocity by the equation $\tau = f\rho u_m^2/2$ (Jonsson, 1967) where ρ is the fluid density and f is an empirically obtained friction factor. Because the friction factor is hard to determine, most investigators present threshold curves using the calculated near-bottom maximum orbital velocity. Komar and Miller (1973) defined the threshold for movement of grains smaller than 0.5 mm with the dimensionless equation:

$$\frac{\rho u_m^2}{(\rho_s - \rho)gD} = 0.21 \left(\frac{d_0}{D}\right)^{1/2} \tag{1}$$

where ρ_s is sediment density and g is the gravitational constant. For quartz sand in water, the relationship $u_m = \frac{\pi d_0}{T}$ gives:

$$u_m = 0.337(g^2 TD)^{1/3} \tag{2}$$

which, in units of centimeters and seconds is equivalent to $33.3\ (TD)^{1/3}$ cm s^{-1} (Clifton, 1976). For movement of grains coarser than 0.5 mm, Komar and Miller define threshold conditions by the dimensionless equation:

$$\frac{\rho u_m^2}{(\rho_s - \rho)gD} = 0.46\ \pi \left(\frac{d_0}{D}\right)^{1/4} \tag{3}$$

which for quartz sand in water reduces to:

$$u_m = 1.395(g^4 TD^3)^{1/7} \tag{4}$$

In units of seconds and centimeters, this is equivalent to $71.4(TD^3)^{1/7}$ cm s^{-1} (Clifton, 1976). The threshold curves of Komar and Miller (1975) for motion of sediment equivalent in density to quartz are based on eqs. 1 and 3 and shown in Fig.4.

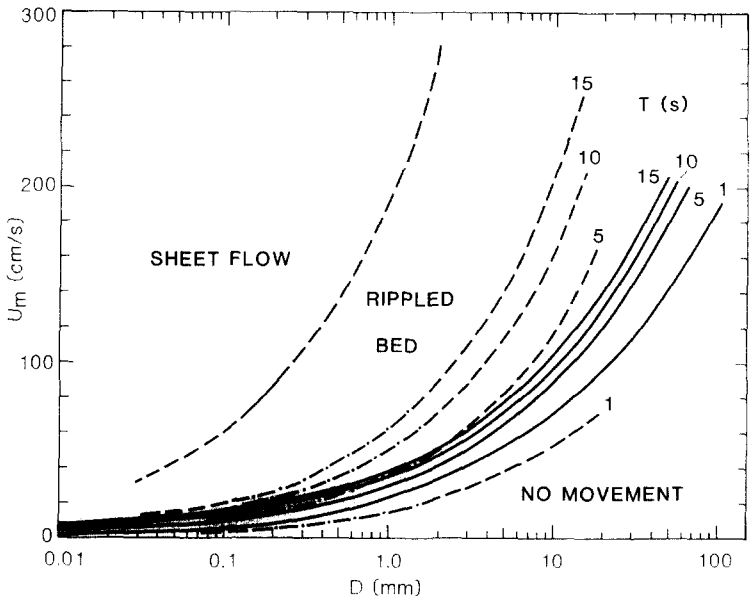

Fig.4. Velocity thresholds for grain movement and sheet flow of quartz sand in water. Solid lines are threshold curves of Komar and Miller (1975) for grain movement. Dashed lines connected by dots are threshold curves of Dingler (1979) in the range of experimental evidence; dots are absent where curves are extrapolated. Threshold curve for sheetflow, from Dingler and Inman (1977), is solid in the size range of experimental evidence and dashed where extrapolated. Note effect of differing wave period on threshold of motion.

Dingler, in a separate experimental study (1979), found that motion for grain sizes between 0.18 and 1.454 mm commenced when the dimensionless criterion:

$$\frac{(\rho_s - \rho)gT^2}{\rho D} = 240\left(\frac{d_0}{D}\right)^{4/3}\left[\frac{\rho(\rho_s - \rho)gD^3}{\mu^2}\right]^{-1/9} \tag{5}$$

is satisfied, where μ is the fluid viscosity and the other terms as defined above. In terms of threshold velocity, eq. 5 reduces to:

$$u_m = 0.052\left[\frac{g^5(\rho_s - \rho)^5}{\rho^4\mu}\right]^{1/6}(TD)^{1/2} \tag{6}$$

which for quartz sand in water, in units of grams, centimeters, and seconds, is equivalent to 52.4 $(TD)^{1/2}$ cm s^{-1} (Clifton, 1976). Threshold curves based on this equation are also shown in Fig.4.

It should be noted that all of the above threshold equations show a dependence on wave period. For any particular grain size a longer period wave requires a higher velocity to initiate grain movement than does a shorter period wave. The basis for this relationship is unresolved. Possibly it derives from the more abrupt onset of flow that occurs under a shorter period wave and the gradient of stress that is associated with greater acceleration.

The threshold curves for onset of grain motion are plotted in Fig.4. In the range of fine sand, the sets of curves are fairly consistent, but they deviate markedly when extrapolated to coarser bed material. Unfortunately, it is the larger size ranges where threshold values are most useful for defining minimum possible wave size and water depth combinations.

Dingler and Inman (1977) determined that sheet flow occurs in fine sand under a relationship whereby $\rho u_m^2/(\rho_s - \rho)gD = 240$. For quartz sand in water this equation reduces to:

$$u_m = 19.9(gD)^{1/2} \tag{7}$$

which, in units of centimeters and seconds is equivalent to $623\, D^{1/2}$ cm s^{-1}.

The threshold curve for sheetflow derived therefrom is shown on Fig.4. It should be noted that this curve was observed only in a narrow range of grain size (0.0128—0.0158 cm) and extrapolation beyond this range must be done with caution.

All the above threshold equations assume spherical grains of uniform size on a flat bed. Bagnold (1963) suggested that sand grains on a previously rippled bed would move at somewhat lower flow velocities, and Southard and Dingler (1971) showed that ripples under unidirectional flow could propagate downstream of a disturbance under subthreshold conditions. Hallermeier (1981) notes that the velocity required to initiate movement over a rippled bed may be half of that required for the same material on a flat bed. In the absence of a definitive study on this problem, reliance must be placed on the flat-bed thresholds noted in the foregoing.

When a range of grain sizes occurs, as is the case outside the laboratory, most people use the median or arithmetic mean diameters, which are easily calculated. Some evidence exists that the effective size for consideration of movement of poorly sorted sediment is less than the median diameter (Hallermeier, 1981). Bagnold (1966) recommended that the geometric mean diameter be used because it more realistically weights the size distribution. Inasmuch as wave-worked sands are typically well-sorted, the median diameter probably suffices.

Threshold values commonly have their greatest use in calculating the forces required to move the coarsest clasts available. In many cases, the size of these largest clasts substantially exceeds that of the bulk of the bed material. The assumption of uniformly sized particles in the foregoing equations casts doubt on their applicability to isolated large clasts on a smaller bed. Fahnestock and Haushild (1962) suggest that isolated cobbles would move under unidirectional flow as easily on a plane sand bed as on a bed of gravel. But would the threshold velocity thereby be significantly reduced? Preliminary experiments in a water-tunnel indicate that the threshold for movement of subspherical quartz grains about 1 cm in diameter on a bed of about 0.05 cm sand is not greatly less than that predicted by Komar and Miller (1975). Under the highest oscillatory velocity possible with the apparatus (85 cm s^{-1} at T = 16 s), the clasts remained immobile (R. August, pers. commun., 1983). According to the curves of Komar and Miller (1975),

threshold velocity of such clasts under 16 s waves is slightly more than 100 cm s^{-1} (Fig.4).

The effect of grain shape on the threshold curve has not been determined. However, using the equivalent sphere diameter is satisfactory in most situations involving terrigenous detrital material. Shelly or other non-spherical biogenic material would almost certainly require different threshold equations.

Relations between ripple spacing and orbital diameter

Two disparate views exist regarding the relation of ripple spacing and orbital diameter. Inman (1957) suggested that for a given grain size, ripple spacing is directly proportional to orbital diameter until some critical maximum orbital diameter is reached, whereupon spacing becomes inversely proportional to orbital diameter, diminishes and ultimately reaches a constant intermediate value. Dingler (1974), plotting both Inman's (1957) field data and original field and laboratory measurements found a similar relationship. In contrast, Allen (1979), after plotting a large amount of existing data (mostly laboratory), found no well-defined relation between orbital diameter and ripple spacing for a given size of sand. He therefore concluded that Inman's bell-shaped curve was spurious. Miller and Komar (1980a), after analysing much of the same data, concluded that there were differences in the data sets that could be attributed to the type of laboratory device used to generate the oscillatory motions. In particular, the results of oscillating bed experiments, which dominate Allen's data, are different from water-tunnel, wave-channel, and presumably, field results. Oscillating bed experiments indicate that, for a given grain size, ripple spacing increases with orbital diameter until it reaches a maximum and then remains constant. Plots of water tunnel and wave channel experiments, in contrast, show a tendency toward the bell-shaped curve (Miller and Komar, 1980a).

Figure 5a is a dimensionless plot of λ/D against d_0/D for a number of field and laboratory studies. Oscillating bed experiments are specifically omitted. The field data tend to dominate the right side of the diagram (high d_0/D values), whereas the laboratory experiments dominate the plot at low d_0/D values. As might be expected the field data are more broadly scattered, but both sets of data show the bell-shaped relationship.

Using a similar plot that incorporated Inman's (1957) and Dingler's (1974) data, Clifton (1976) subdivided symmetric ripples into three types based on the relationship between ripple spacing and orbital diameter. This subdivision (Fig.5b) appears to be valid for the larger data set presented here in Fig.5a.

Orbital ripples are those on the left side of Fig.5b where ripple spacing is proportional to orbital diameter in the approximate relationship (Miller and Komar, 1980a):

$$\lambda = 0.65\, d_0 \tag{8}$$

Such ripples can form under conditions where the d_0/D ratio lies in the range of 100—3000 or more (Fig.5b). Their spacing-to-grain-size ratio (λ/D)

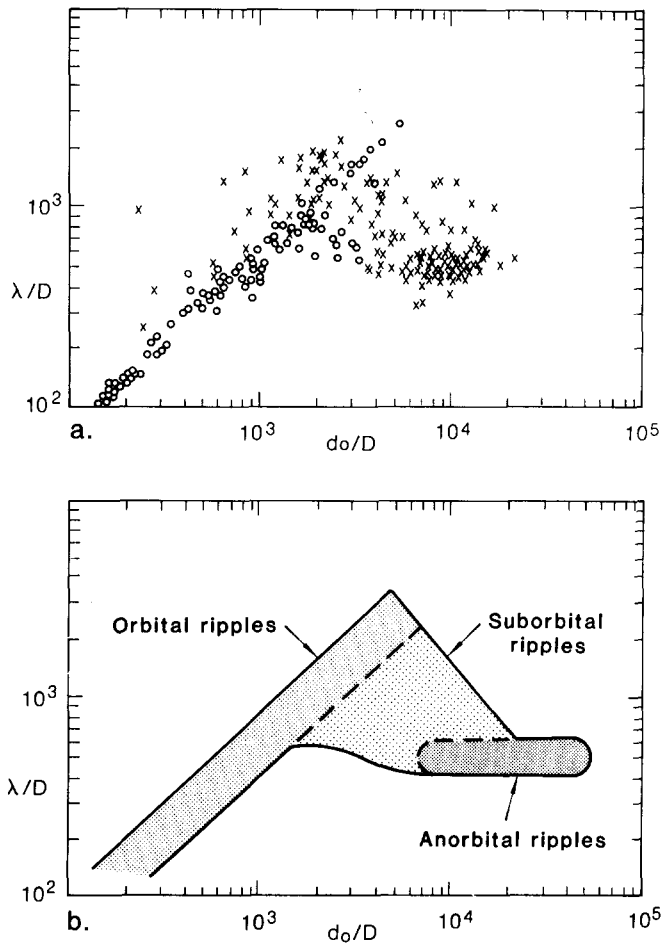

Fig.5. *a.* Plot of ratio of ripple spacing to grain size against ratio of orbital diameter to grain size. Data include field observations (crosses) and experimental (wave channel, water tunnel) data (circles). Field data from Inman (1957), Dingler (1974), Miller and Komar (1980b) and Dingler and Clifton (this volume). Experimental data from Carstens et al. (1969), Mogridge and Kamphuis (1972), and Miller and Komar (1980a). *b.* Classification of ripples based on the distribution shown in *a.*

ranges from less than 100 to more than 2000. Because of the requirement for short oscillatory motion, orbital ripples occur most commonly in very shallow water under short-period waves. Long-period waves can generate similarly short orbital flow at the bottom in deeper water, but because of the relationship $u_m = \pi d_0/T$, the velocity will be reduced and threshold conditions less likely to be reached. The spacing of orbital ripples tends to increase in a shoreward direction, paralleling the increase in d_0 as a wave shoals (Komar, 1974). The spacing appears to be independent of grain size.

Ripple spacing remains proportional to orbital diameter until the d_0/D ratio reaches the range of 1000—3000 (Clifton, 1976, and calculations from

Miller and Komar, 1980a). Under such conditions (Fig.5b), the ripple spacing decreases as orbital diameter increases. Ripples formed under these conditions were accordingly termed "suborbital" (Clifton, 1976). The ripple spacing appears to depend both on orbital diameter and grain size in some undefined relationship.

At d_0/D values in excess of 5000, ripple spacing stabilizes at a value that is independent of orbital diameter (Fig.5b). Termed "anorbital ripples" by Clifton (1976), such ripples are most commonly observed in fine sand where they have a spacing of 5—10 cm. Typically their λ/D ratio lies in the range of 400—600 under conditions of a single train of waves. Recent field studies indicate that, under a polymodal wave spectrum (more than one wave train present), the spacing-to-grain size ratio of anorbital ripples may be on the order of 1200 (Miller and Komar, 1980b). Anorbital ripples are probably the only type to form in fine sand under very long period (>12 s) waves (assuming a threshold velocity of 15 cm s^{-1} for sand 0.125 mm in median diameter, a 12 s wave will induce a threshold orbital diameter of nearly 60 cm, and a d_0/D ratio of 4800). Anorbital ripples include the "reversing" ripples described by Inman (1957), which alternate their direction of asymmetry with each reversal of the oscillatory flow.

An intriguing relation exists between anorbital ripples and the "maximum ripples" produced by an oscillating bed. Both have been described using the dimensional parameter $\lambda/D^{1/2} \simeq 60$ $cm^{1/2}$ (Clifton, 1976, for anorbital ripples; Bagnold, 1946, for "maximum" or "natural pitch" ripples). If this relationship is not entirely coincidental, it may provide insight into a fundamental difference between ripples formed on an oscillating bed and those formed under oscillating fluid. Both ultimately generate ripples for which the spacing is independent of orbital diameter and can be defined as $\lambda \simeq 60\, D^{1/2}$ if both λ and D are in cm. Ripples on oscillating beds reach this spacing by continuously increasing their size; ripples formed by fluid motion such as those occurring in nature seem to have the potential to grow as orbital ripples beyond the size of the maximum ripple of the oscillating bed. Miller and Komar (1980a) suggest that this growth ceases at the point whereby $\lambda = 14.7\, D^{1.68} \times 10^3$ (both λ and D measured in cm). Further increase in orbital diameter causes the spacing to shrink (suborbital ripples) until the "natural pitch" is achieved (anorbital ripples).

Except for reversing ripples, the relationships between λ and d_0 described in the foregoing paragraphs appear to be valid only for symmetrical ripples. The spacing of asymmetric ripples appears to follow a different pattern, which remains to be resolved (Clifton, 1976). The continuum that appears to exist between small and large symmetric bedforms is lacking for asymmetric bedforms. The marked difference in size between wave-formed lunate megaripples and associated long-crested asymmetric ripples near the high-energy surf zone (Clifton et al., 1971) suggests a discontinuity in the scale of asymmetric wave-formed bedforms similar to that within the lower regime of unidirectional flow.

Nielsen (1981) relates ripple spacing to a "mobility number" ψ (Brebner, 1981) that is equivalent to the relative stress of Komar and Miller (1972)

$(\pi d_0/T)^2 \rho/(\rho_s - \rho)gD$. Nielsen proposes that the spacing of naturally occurring ripples is best described by the equation:

$$\lambda = \frac{d_0}{2} \exp\left(\frac{693 - 0.37 \ln^8 \psi}{1000 + 0.75 \ln^7 \psi}\right) \tag{9}$$

This expression is complicated by the presence of three variables (d_0, D, T), but can be solved as a set of curves relating λ and d_0 for a specific grain size (Fig.6) or a specific wave period. As shown in Fig.6, Nielsen's equation predicts a λ/d_0 relation similar to that described by Inman (1957) and Dingler (1974) in which orbital, suborbital and anorbital ripples can be readily identified. It should be noted that on this diagram, the ripple type is no longer simply a function of d_0/D. Nielsen (1981) suggested that the spacing of ripples formed in the laboratory follows a somewhat different pattern (Fig.7) indicated by the equation:

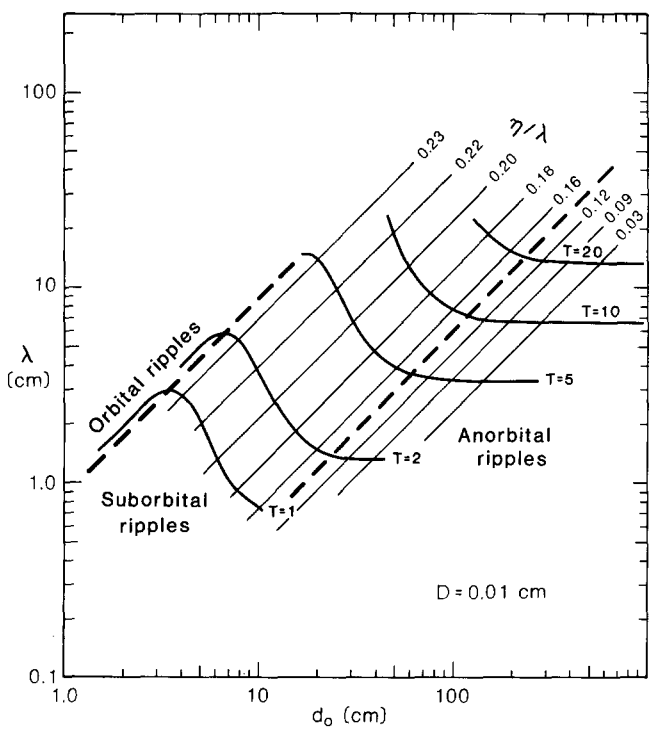

Fig.6. Plot of spacing of naturally occurring quartz sand (D = 0.01 cm) ripples against orbital diameter for waves of different period based on eq. 9 (Nielsen, 1981). The curve representing the indicated wave period is terminated on the left side of the diagram at the threshold orbital diameter (using eq. 19) and on the right side of the diagram at the maximum possible orbital diameter (using a combination of Fig.9 and eq. 16). Fields for orbital, suborbital and anorbital ripples are indicated as a function of the nature of the relation between spacing and orbital diameter. Lines of equal ripple steepness (λ/η) are drawn based on eq. 11 (Nielsen, 1981). Data set includes no waves with periods less than 6 s.

$$\lambda = \frac{d_o}{2}(2.2 - 0.345\,\psi^{0.34}) \qquad (10)$$

This equation is of limited validity at larger values of ψ, where the corresponding values of λ become negative (see Fig.7). The difference between the spacing relations of naturally occurring and laboratory ripples is attributed without elaboration to the irregularity of natural waves (Nielsen, 1981).

The question of the influence of wave period on ripple spacing remains unresolved. Bagnold's (1949) statement that, in all of his experimental studies, the pitch (spacing) was independent of the speed of oscillation implies that period was not a factor. The spacing of anorbital ripples described by Miller and Komar (1980b) does not change significantly under unimodal waves of periods that ranged from 8 to 16 s. Nonetheless, as noted before, they found that the spacing of anorbital ripples under a polymodal wave spectrum was more than twice that of ripples formed in sand of the same size under unimodal waves of similar periods. On the basis of experimental evidence, Nielsen (1981) suggests that spacing depends on wave period, particularly at the shorter periods (in the range of 1—2 s). Nielsen's expression for the spacing of naturally occurring ripples (eq. 9) contains wave period as a variable, the effect of which can be seen in Fig. 6. It should be noted, however, that the data base from which Nielsen derives his expression contains no

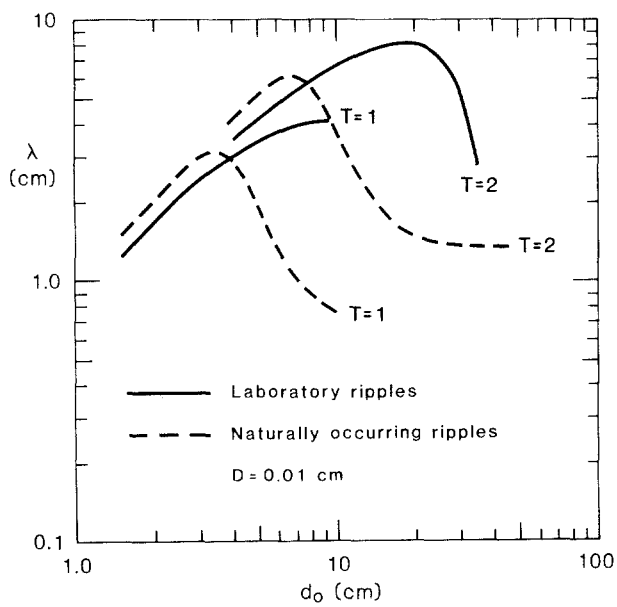

Fig.7. Comparison of spacing-orbital diameter relations for laboratory and naturally occurring ripples in quartz sand (D = 0.01 cm) under waves with periods of 1 and 2 s using eqs. 9 and 10 (Nielsen, 1981). Curves drawn for naturally occurring waves are suspect because of the absence of data for waves of 1 and 2 s. Curve for laboratory ripples formed under 2-s waves is suspect at the higher values of d_0 where it begins a precipitous decline.

waves with periods of less than 6 s. For waves of shorter period, the relation based on laboratory ripples (Fig. 7) may be of greater validity, particularly at the less extreme values of d_0 for waves of a given period.

In summary, field observations and laboratory experiments using wave channels and water tunnels suggest that orbital diameter can be estimated from the ratio of ripple spacing to grain size, both readily measured parameters. At λ/D values less than 400, ripple spacing seems to depend on orbital diameter in the approximate relationship $\lambda = 0.65\, d_0$ (orbital ripples). A ratio in the range of λ/D = 400—600 indicates either orbital ripples or anorbital ripples ($d_0 > 5000\, D$). Spacing-to-grain size ratios in excess of 600 suggest either orbital ripples or suborbital ripples (d_0 = 1000—5000 D). Where the type of ripple is ambiguous (orbital or anorbital, orbital or suborbital), the complete process of interpretation may indicate which is more likely. Orbital diameter cannot presently be estimated from the spacing-to-grain size relationship of asymmetric wave-formed ripples. Variation in wave period may further complicate the interpretive process in ways that are not yet fully understood.

Relations between ripple steepness and orbital diameter

Another approach to determining orbital diameter is based on the ratio of ripple height to wavelength (η/λ) or ripple steepness. Several investigators have described three types of asymmetrical ripples based on steepness: rolling-grain ripples, vortex ripples, and post-vortex ripples. Bagnold (1946) gave the name rolling-grain ripples to low-amplitude ripples that form on flat beds under oscillatory flows just above the threshold for grain motion. Sleath (1976) and Allen (1979) apply this name to all low-amplitude, wave-generated ripples. The steepness (η/λ) of rolling-grain ripples ranges from zero to about 0.12 (a VFI or λ/η of about 8; Allen, 1979); they are too low in amplitude for a vortex to form in the ripple troughs. At least in the lower part of the ripple regime these ripples are metastable; they readily convert to vortex ripples if there are many large disturbances on the bed or if the flow velocity increases. The discussion by Miller and Komar (1980a) suggests that rolling-grain ripples are stable bedforms only on oscillating beds.

Vortex ripples occupy much of the ripple regime under oscillating fluid, extending from near the threshold of grain motion to near the onset of sheet flow (Miller and Komar, 1980). The large, sediment-laden vortex, which forms in the lee of each crest, gives these ripples their name (Bagnold, 1946). Ripple steepness is essentially constant throughout the ripple regime, having a typical value of about 0.15 (Dingler and Inman, 1977) and a range of about 0.12—0.22 (or VFI between 4.5 and 8; Bagnold, 1946).

As flow velocity increases over the vortex ripples, a point is reached where sand is stripped from the ripple crests. Orbital diameters are very large when this velocity is attained, and the ripple wavelength is unchanged by increasing flow. The net result is post-vortex ripples (Dingler and Inman, 1977) or rolling-grain ripples (Allen, 1979) that show a systematic decrease in ripple steepness from 0.15 to 0 as sheet flow conditions are approached (Dingler and Inman, 1977).

The relationship between ripple steepness and ripple spacing for given values of orbital diameter and sediment grain size is not completely clear. Several workers (Allen, 1979; Allen, 1981a, b) equate vortex ripples with orbital ripples. By this interpretation, ripples that have steepness values in the range of 0.12—0.20 can be used to calculate orbital diameter from eq. 8. This approach may be overly simplistic, however. A plot of field and wave tank data (Fig.8) indicates that vortex ripples ($\eta/\lambda > 0.1$) exist for d_0/D values of less than 5000. This plot confirms that orbital ripples ($d_0/D < 1000$) are vortex ripples, but demonstrates that the converse may not be true. Vortex ripples also form at d_0/D values of 1000—5000, where ripple spacing may be inversely related to orbital diameter. Post-vortex ripples appear to be stable only under conditions where anorbital ripples form, and therefore indicative of d_0/D values >5000.

Nielsen (1981) proposes that ripple steepness, like spacing, is a function of the mobility number ψ. Using the same data set as incorporated into Fig.7, he suggests that for naturally occurring ripples,

$$\eta/\lambda = 0.342 - 0.34(1/2\, f_w \psi)^{1/4} \qquad (11)$$

where f_w is a friction factor equivalent to $\exp[5.213\,(5D/d_0)^{0.194} - 5.977]$. Curves of equal steepness for ripples in quartz sand 0.01 cm in diameter on Fig.6 also indicate that the transition from vortex to post-vortex ripples (in the range of $\eta/\lambda = 0.12$) accompanies the transition to anorbital ripples.

It should be noted that the steepness of vortex ripples may be reduced by faunal activity, compaction, or other post-depositional processes (Reineck and Wunderlich, 1968; Boersma, 1970; Allen, 1981a). Therefore, low values of ripple steepness may not necessarily reflect anorbital conditions. For

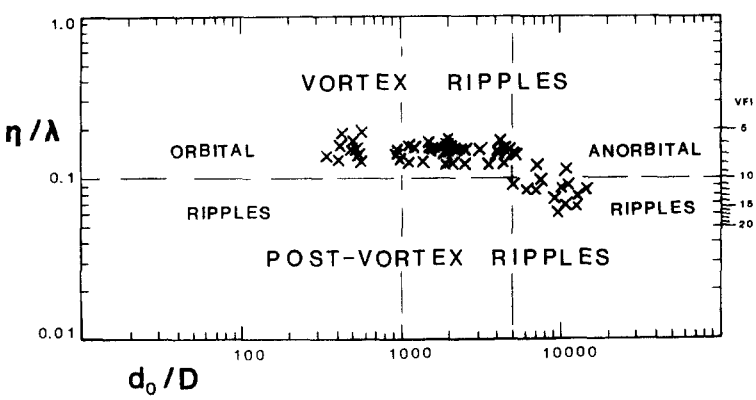

Fig.8. Plot of ripple steepness (η/λ) against the orbital diameter to grain size ratio (d_0/D), showing the relationship between vortex and post-vortex ripples (defined by ripple steepness) and orbital and anorbital ripples (defined by the d_0/D ratio). Vertical form index (VFI) scale on right side of plot. Ripples with $d_0/D < 1000$ are assumed to be orbital; those with d_0/D ratios >5000 are assumed to be anorbital. Ripples with d_0/D ratios between 1000 and 5000 are considered to be transitional between orbital and anorbital ripples (suborbital ripples). Data from Inman (1957) and Dingler (1974).

these reasons, we feel that ripple steepness by itself presently is not a reliable indicator of orbital diameter in ancient deposits.

Asymmetry of bedforms

Little is known about the degree of orbital velocity asymmetry that is required to generate asymmetric bedforms. Clifton (1976) used several lines of reasoning to suggest that a velocity—magnitude difference Δu_m of a few centimeters per second could produce asymmetry in small ripples, and Allen (1979) concluded that the degree of ripple asymmetry is proportional to the ratio of the wave-drift velocity to the near-bottom velocity maximum. This conclusion is highly tentative and virtually no data exist regarding the nature of flow that causes asymmetry of larger ripples or wave-formed lunate megaripples (which, as noted in the foregoing, have been observed to migrate in the absence of an observable wave-drift current). Tietze (1978) produced asymmetric ripples in a small experimental wave tank under measured Δu_m values between 1 and 11 cm s^{-1}. He demonstrates a relationship between the degree of ripple asymmetry and the ratio between drift velocity and maximum orbital velocity, but does not indicate where in the water column the net drift was measured. His observation that ripple asymmetry is increased by adding coarse sand to the bed strongly suggests an influence by velocity—magnitude asymmetry rather than by net drift (Kemp, 1975). Field observations show that shoreward-facing, wave-induced asymmetry of bedforms is most common in shallow water near the breaker zone (Davidson-Arnott and Greenwood, 1974; Clifton, 1976). Without a documented relationship, however, between ripple shape and some measure of flow asymmetry, quantitative estimates of the paleo-asymmetry of oscillatory flow are presently questionable.

STEP 2. ESTIMATING POSSIBLE COMBINATIONS OF WAVE PARAMETERS AND WATER DEPTHS FROM FLOW PARAMETERS

Once flow parameters, such as orbital diameter or maximum velocity, have been derived from the sedimentary structures, a range of wave conditions and water depths can be estimated. The normal complexity of the sea surface forces an investigator to undertake a great deal of simplification; commonly a "typical wave form" is identified that can be represented by mathematical equations from an appropriate wave theory. Such simple waves can be approximated in experimental studies. Spectral analysis provides a more accurate approach to describing natural waves (Dingler, 1974; Miller and Komar, 1980b; Dingler and Clifton, 1984, this volume). It is worth noting that a complicated wave field, composed of several different trains of waves can profoundly influence the development of bedforms (Clifton et al., 1971; Miller and Komar, 1980b).

Various wave theories can be used to relate flow parameters to basic wave parameters. The four most commonly cited are the: (1) Airy; (2) Stokes; (3)

cnoidal; and (4) solitary wave theories. Each is most applicable under a specific set of conditions of wave height, wave period and water depth (Fig. 9). Each has associated disadvantages and each should be considered only an approximation. A brief description of these theories is presented here; for further information, the reader is directed to the useful summary provided by Komar (1976).

Airy theory, which treats waves as sinusoidal forms, is the simplest in application. It is applicable to small amplitude waves in a wide range of water depths (relative to wave length) and provides for reasonable approximation of measured orbital diameter and near-bottom maximum velocities for real waves in shallow water (LeMehaute et al., 1969). It does not, however, provide for asymmetric flows.

The other theories noted above apply to waves with peaked crests and flattened troughs, a shoaling transformation of the sinusoidal wave. All predict asymmetric oscillatory motion. The Stokes wave theory is relatively simple, but, according to Komar (1976), becomes inaccurate for large waves when extended into shallow water. Figure 10 indicates the combinations of water depth and wave height under which the Airy and Stokes theories apply for waves of different periods using the criterion employed by Komar (1976) whereby the expression $HL^2/h^3 = 32\ \pi^{2/3}$ defines the boundary between cnoidal and Airy or Stokes waves, and $H/L = 0.0625 \tanh (2\pi h/L)$ defines the boundary between Airy and Stokes waves. This figure shows, for example, that the Stokes wave theory can describe wave form and water motions for a 10 s wave in 3 m of water, provided the wave height does not exceed 1 m. It should be noted that in water depths greater than about 7 m, cnoidal wave theory does not apply regardless of wave height. At greater depths and/or

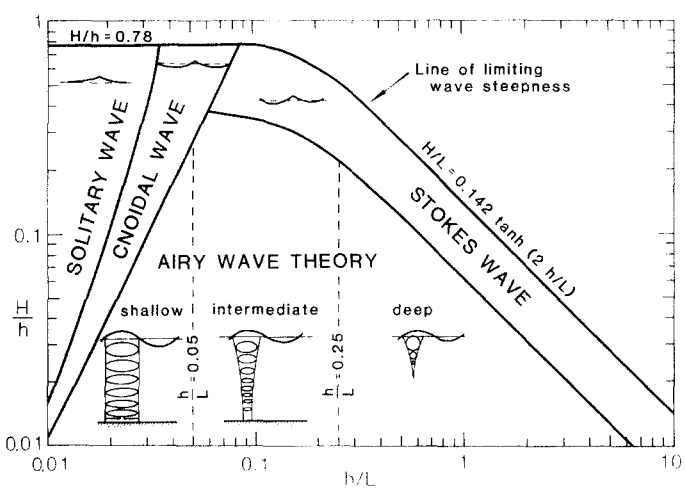

Fig.9. Conditions of wave length (L), wave height (H) and water depth (h) for which different wave theories are most applicable (from Komar, 1976). Approximate theoretical waveform shown within each field.

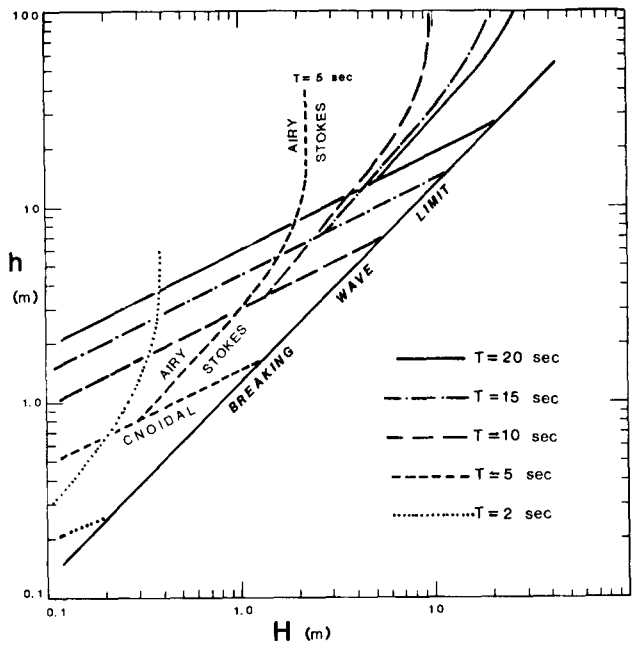

Fig.10. Areas of applicability (in terms of water depth and wave height) for Airy, Stokes, and cnoidal wave theories for waves of different period. Limiting relations shown for 5-s wave are similar for the waves of other periods. Limits between Stokes and Airy theory defined by $H/L = 0.0625 \tanh (2\pi h/L)$ and between Stokes-Airy and cnoidal theory by $HL^2/h^3 = 32\pi^{2/3}$ (Komar, 1976).

smaller waves, the less cumbersome Airy theory provides an equally valid approximation.

Cnoidal wave theory may be more accurate than Stokes theory for large waves in shallow waters (Wiegel, 1960), but its complexity severely limits its use. In many cases the Stokes or Airy theory may sufficiently approximate the water motion under conditions where cnoidal wave theory is otherwise indicated (Komar, 1976, p.62).

Solitary waves are individual progressive waves composed of a single crest. Waves very close to shore commonly resemble the solitary wave shape although such waves can be described by their wavelength and period, terms that are not appropriate for true solitary waves. Although solitary wave theory is relatively accessible, it does not truly describe periodic oscillatory motion of real wind-generated waves. This and the deviation of predicted results from measured parameters casts doubt on the use of solitary wave theory for nearshore studies (Komar, 1976, p.59).

Wave length and period

The flow parameters described in Step One (u_m, d_0, etc.) result from different combinations of wave size, shape, and water depth. The size of a

wave is most readily perceived in terms of its height H and length L (Fig.1). The significant wave height (average of the highest 1/3 of the waves) is often used to represent a wave field (Dingler, 1974), even though the root-mean-square wave height is naturally associated with spectral analysis. The length of a wave is a variable parameter inasmuch as it changes significantly as a wave shoals. The wave period T, the time required for one oscillation, is related to the wave length by $T = L/C$, where C is the phase velocity (velocity of propagation) of the wave in question. Both phase velocity and wave length decrease progressively at the same rate as a wave shoals. The wave period remains unchanged and is therefore a more useful description of a wave than either length or velocity of propagation.

Airy wave theory relates the length of a given wave to its period and to the water depth h by the equation:

$$L = \frac{gT^2}{2\pi} \tanh\left(\frac{2\pi h}{L}\right) \tag{12}$$

Equation 12 can be simplified in deep water ($h/L_0 > 1/4$) where the hyperbolic term approaches unity:

$$L_0 = \frac{gT^2}{2\pi} \tag{13}$$

or, in mks units, $L_0 = 1.56\ T^2$ m. This relationship implies that, for waves of any period, there is an associated, easily calculated deep-water wave length. The deep-water wave length can be introduced into eq. 12 whereby:

$$L = L_0 \tanh(kh) \tag{14}$$

where k, the wave number, equals $2\pi/L$. Expressed this way, the hyperbolic term can be viewed as a shoaling factor that is applied to the deep-water wave length to give the wave length at any water depth. Equation 14, however, remains complicated by the presence of the unknown (L) on both sides of the equation.

This problem can be resolved by dividing both sides of eq. 14 by the water depth h and rearranging such that:

$$\frac{h}{L_0} = \frac{h}{L} \tanh(kh) \tag{15}$$

This expression has been solved by Wiegel (1954) and presented in tabular form in the Shore Protection Manual (U.S. Army Coastal Engineering Research Center, 1973). Using these tables the solution of many of the wave equations is greatly simplified. For any ratio of water depth to deep-water wave length (or, by inference, any combination of water depth and wave period), the tables indicate the corresponding values of h/L, kh, the different hyperbolic and trigonometric functions of (kh), and other parameters. Such relations allow the wave size at any water depth to be readily expressed in terms of wave height and wave period.

Wave height

Some natural limits to wave height provide useful constraints to the combination of solutions possible from the wave equations. One such limit occurs in shallow water whereby waves become unstable and break at some critical water depth. The ratio of wave height to water depth at which breaking occurs depends on the beach slope and the initial wave steepness (Iverson, 1952). A value of 0.78 has been most widely accepted for this ratio (Komar, 1976). In deeper water, waves will break if their height exceeds the value $L/7$ (Miche, 1944). Although the largest possible wind wave could theoretically exceed 65 m in height (Bascom, 1980, p.58), the largest recorded remains the 34-m wave observed from the U.S.S. "Ramapo" in 1933. Accordingly, 40 m seems a reasonable maximum height for a set of wind-generated waves. Figure 11 illustrates the maximum stable height for waves of different periods.

Orbital diameter and maximum velocity

In Airy wave theory the orbital diameter at the sea floor d_0 is:

$$d_0 = \frac{H}{\sinh(kh)} \tag{16}$$

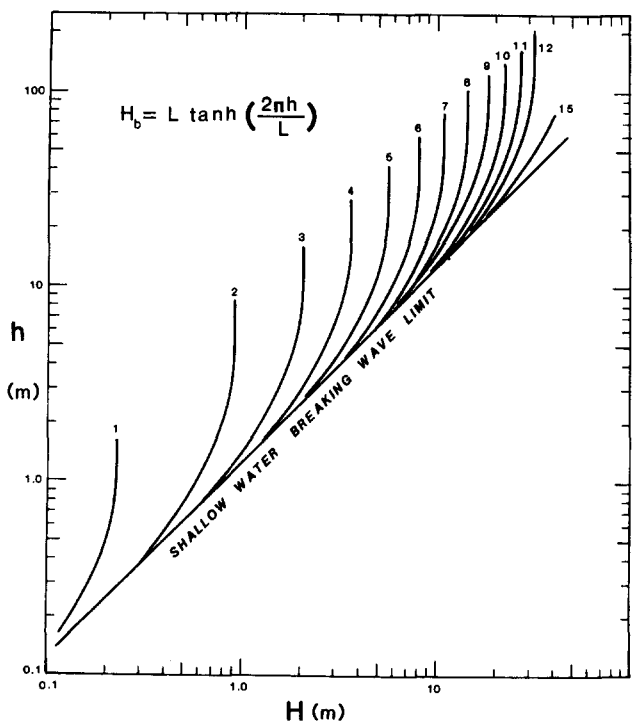

Fig.11. Maximum wave height (H) for waves of different period as a function of water depth. Curves for waves of different period terminate at approximately $h = L_0$ (= 1.56 T^2 m).

and the maximum orbital velocity at the seafloor u_m under the crest of the wave is:

$$u_m = \frac{\pi d_0}{T} = \frac{\pi H}{T \sinh (kh)} \tag{17}$$

The velocity under the trough of an Airy wave is of similar magnitude but opposite in direction. Although Airy theory is specifically applicable to conditions of relatively small waves in deep water, LeMehaute et al. (1969) showed that it provides a reasonable approximation to measured orbital diameters and near-bottom maximum velocities for finite amplitude waves in shallow water. Equations 16 and 17 are valuable for calculating the combinations of wave height, period, and water depth that will generate a particular wave-formed bedform or internal structure. One can recast these equations in terms of wave height

$$H = d_0 \sinh (kh) = \frac{u_m T \sinh (kh)}{\pi} \tag{18}$$

and then, using the structurally indicated value of d_0 or u_m, solve the equation for a series of selected water depths under waves of several different periods. In these calculations (shown in more detail in the first example, following), the chosen combination of wave period and water depth determines the value of h/L_0 (equal to $h/1.56\ T^2$ in meters), which then can be used to enter the wave tables to compute the appropriate value of h/L. The results can then be plotted as curves of equal wave period on an "H—h" (wave height vs. water depth) diagram. Figure 12 is an example of an H–h diagram that shows the combinations of wave height and water depth required to produce sheet flow in medium-grained sand under waves of several different periods.

One can also combine estimates of orbital diameter with those of threshold velocity to determine the maximum wave period that can produce the given combination. Longer period waves are capable of generating the same orbital diameter in deeper water, but the orbital velocities will be reduced below threshold level. Dingler (1979) combines his threshold equation for grain movement of quartz sand with the relation $u_m = \pi d_0/T$ (all measurements in cm and s) to derive the expression for maximum or threshold wave period:

$$T = 0.17(d_0^2/D)^{1/3} s \tag{19}$$

The threshold equations of Komar and Miller (1975) provide for similar expressions of threshold wave period (in units of cm and s):

$$T = 0.17 \left(\frac{d_0^3}{D}\right)^{1/4} s \qquad (\text{for } D < 0.05 \text{ cm}) \tag{20}$$

$$T = 0.065 \left(\frac{d_0^7}{D^3}\right)^{1/8} s \qquad (\text{for } D > 0.05 \text{ cm}) \tag{21}$$

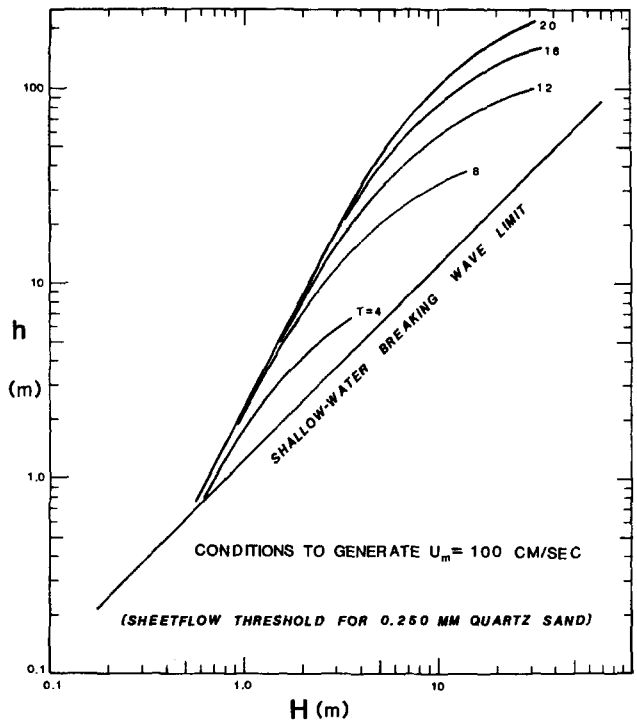

Fig.12. Combinations of wave height and water depth that will generate sheetflow of 0.250 mm quartz sand (u_m = 100 cm s^{-1}) under waves of different period. Curves for waves terminated at maximum stable wave height.

Velocity asymmetry

As noted in the foregoing section, the Airy theory cannot provide estimates of velocity asymmetry, and a higher order theory must be invoked. Stokes second-order theory provides the easiest calculable estimate of velocity asymmetry in shallow-water. Asymmetries can be calculated from the other shallow-water wave equations, but their inherent complexity generally limits their application in paleoenvironmental interpretations.

Stokes' (1847) solution for waves of finite height results in water-particle motion that is asymmetric with respect to both maximum velocity and time. The velocity of the water moving forward under the wave crests exceeds the reverse velocity under the wave trough. The duration of forward flow is less than that of the reverse flow, but the net result is an onshore migration of the water particles.

Stokes second-order wave theory provided equations both for velocity-magnitude asymmetry and for the net drift velocity of the water particles. The complete equation for near-bottom orbital velocity under the crest of a Stokes wave is:

$$u_m^c = \frac{\pi H}{T \sinh(kh)} + 3/4 \left[\frac{(\pi H)^2}{LT \sinh^4(kh)}\right] \tag{22}$$

whereas that under the trough of the wave is:

$$u_m^t = -\left[\frac{\pi H}{T \sinh(kh)}\right] + 3/4 \left[\frac{(\pi H)^2}{LT \sinh^4(kh)}\right] \tag{23}$$

The first term in eqs. 22 and 23 is the expression for maximum orbital velocity under an Airy wave; the second term can be viewed as a correction factor imposed by the Stokes wave. Clifton's (1976) expression for velocity magnitudes asymmetry is the sum of eqs. 22 and 23 (in effect, twice the correction factor):

$$\Delta u_m = \frac{3(\pi H)^2}{2\,LT \sinh^4(kh)} = \frac{14.8\,H^2}{LT \sinh^4(kh)} \tag{24}$$

The net drift velocity $\overline{U}$ generated by a Stokes wave is derived by integrating (over a wave period) the Stokes second-order equation for water particle displacement. The result involves assumptions (infinite channel length, constant depth, absence of viscosity) that are inappropriate for most natural situations. Accordingly, Longuet-Higgins (1953) developed a wave drift relationship for the case of a Stokes wave in a channel of finite length with a real viscous fluid. The resulting equation:

$$\overline{U} = \frac{5(\pi H)^2}{4\,LT \sinh^2(kh)} \tag{25}$$

describes a slow onshore mass transport of water due to wave passage.

Unfortunately, as noted previously, neither Δu_m nor $\overline{U}$ as defined in eqs. 24 and 25 is completely satisfactory for expressing the velocity asymmetry imparted by shoaling waves. Compounding this problem is the fact that the Stokes second-order equation can be of uncertain validity at the shallow, near-breaker-zone depths where asymmetry of flow is most important. Unfortunately, cnoidal wave theory is generally too complicated for geologic application and solitary wave theory has been shown to be unreliable under real conditions (Komar, 1976, p.59). It thus appears that, despite its obvious importance in determining bedform shape and sediment transport, there presently is no satisfactory means of quantitatively estimating velocity asymmetry.

STEP 3. DERIVING PALEOENVIRONMENT INTERPRETATIONS FROM INFERRED COMBINATIONS OF WAVE CHARACTER AND WATER DEPTH

Typically, the results of an analysis of ancient, wave-generated structures take the form of an H—h diagram on which are plotted the various combinations of wave height, period and water depth that will generate a particular flow parameter. Commonly, these combinations span a broad range of water depth and wave size. To apply these data to a paleoenvironmental problem

requires that the combinations be restricted to a smaller range. The natural limits to wave height described in the foregoing section provide one such restriction. Further constraints can be placed by an application of wave hindcasting techniques, geological reasoning, or a combination of the two. Wave hindcasting is a technique for estimating the height and period of waves on the basis of past speeds and duration of winds, fetch length and water depth. (Shore Protection Manual, U.S. Army Corps of Engineers Coastal Research Center, 1973). The inferred period and height of ancient waves can be thus related to basin size and wind speed and direction. Paleogeographic reconstruction may thereby impose limits on the waves, or conversely, the reconstructed waves may indicate size and shape of the depositional basin.

Geological evidence can also place constraints on water depth. Evidence for water depth may be drawn from paleoecologic analyses, the nature of associated facies, or the vertical distance to the inferred base-of-beach in a prograding shoreline deposit (see Dupré, 1984, this volume). Directional features may indicate the direction of wave approach relative to the shoreline and the presence of wave-driven currents near the shoreline. The use of geological reasoning is limited only by the availability of critical data and the resourcefulness of the investigator.

EXAMPLES

The following examples illustrate different ways in which wave-formed structures can be used to interpret aspects of the paleoenvironment. In each case the procedure is outlined in detail, noting particularly each of the three steps involved.

Example 1. Estimating wave size from threshold velocity

This example has been published (Hunter and Clifton, 1982) but is included here for analysis and to illustrate the procedure. The problem is determining whether or not storm waves were involved in the formation of hummocky cross-stratification in sandstone of Late Cretaceous age exposed at Cape Sebastian on the coast of southern Oregon. The hummocky cross-stratification occurs in the lower part of sediment cycles typically tens of centimeters thick. The hummocky cross-stratified sandstone overlies an erosional surface and grades upward into horizontally stratified sandstone that in turn grades upward into thoroughly bioturbated sandstone. The cycles are composed of slightly graded fine sand. Small pebbles are scattered in the hummocky cross-stratified sandstone and a few lie within the overlying horizontally stratified sand. Exposures of bedding surfaces of the horizontally stratified sandstone commonly show straight-crested symmetrical ripple marks.

The largest pebble, about 5 cm in diameter, found in the horizontally stratified sandstone forms the basis for the calculations presented here. The common presence of symmetrical ripple marks in this facies implies the

presence of waves, which suggests the possibility of using the threshold for movement to calculate maximum orbital velocity.

Step 1. The threshold velocity for moving a 5 cm pebble can be estimated from Fig.4. The curves of Komar and Miller (1975) provide a more conservative value at wave periods larger than 5 s and are therefore employed. These curves indicate an orbital velocity on the order of 200 cm s^{-1}. It should be noted that the fact that the pebble moved on a bed of fine sand rather than on a bed of similarly sized pebbles (assumed for the threshold curves) introduces a measure of uncertainty.

Step 2. To determine the combination of wave size and water depth that would produce the orbital velocity derived in Step 1 requires selection of the appropriate wave theory. Since asymmetry of flow is not involved, Airy theory should provide for reasonable calculations based on the indicated maximum orbital velocity using eq. 18. A table can subsequently be constructed to determine the wave height that at given water depths will generate an orbital velocity of 200 cm s^{-1}. Table I, for example, indicates the wave heights that will generate this orbital velocity at a variety of water depths for a 12-s wave. Similar tables can be constructed for waves of other periods and the results plotted on an H—h diagram (Fig.13) that indicates the combination of water depth and wave height at which waves of several specific periods will generate a near-bottom maximum orbital velocity of 200 cm s^{-1}. Note that the curves for the waves of smaller period are terminated at their maximum stable wave height.

Step 3. Figure 13 indicates that the specified orbital velocity of 200 cm s^{-1} can be generated by waves of widely varying size. Constraints, however, can be imposed by geologic reasoning. The absence of unidirectional crossbedding and shoreline progradational sequences from the cyclic part of the Upper Cretaceous sandstone at Cape Sebastian led Hunter and Clifton (1982) to conclude that deposition did not occur in very shallow water close to a

TABLE I

Computation of wave heights (H) required to generate u_m = 2.0 m s^{-1} at various water depths (h) under a 12 s wave, using Airy wave theory (eq. 18). $L_0 = 1.56\,T^2\text{m} = 225$ m; $H\text{m} = 0.142\,L_0 \doteq 32$ m

h[1]	h/L_0[2]	$\sinh\left(\frac{2\pi h}{L}\right)^3$	H[4]
5	0.022	0.390	3.0
10	0.044	0.579	4.4
20	0.089	0.922	7.0
30	0.133	1.27	9.7
50	0.222	2.21	17.0
70	0.311	3.72	28.0
100	0.444	8.27	63.0

[1]Selected arbitrarily; [2]calculated from indicated values; [3]computed from Wave Data tables (U.S. Army Coastal Engineering Research Center, 1973); [4]calculated from eq. 18.

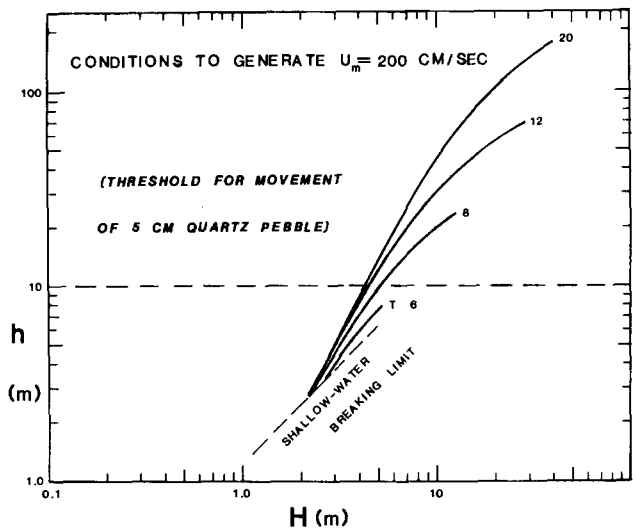

Fig.13. Combinations of wave height and water depth at which a 5-cm quartz pebble will move (estimated u_m = 200 cm s^{-1}) under waves of different period. Curves of waves terminated at maximum stable wave height.

shoreline. Accordingly, they felt that a depth of 10 m was a conservative minimum for deposition of this part of the unit. Applying this limit to Fig.13 eliminates the shorter period waves and implies wave heights of at least 4 m. Since these conditions presumably prevailed during the waning phase of the event that created the sedimentary cycle, even larger waves attended the development of the hummocky cross-stratified sandstone.

Example 2. Determining depositional environment on the basis of grain size and ripple spacing

The Berea Sandstone is a paralic deposit of Mississippian Age that crops out in a north-south belt across the state of Ohio (Pepper et al., 1954; Coogan et al., 1982). In exposures southeast of the city of Cleveland the unit consists of fine sandstone in which sets of trough crossbedding 1—3 m thick alternate with thin (typically less than 1 m thick) sequences of flat-bedded or wavy-bedded sandstone. Bedding surfaces of the flat- or wavy-bedded sandstone commonly exhibit small symmetrical ripple marks. The crossbeds dip to the west and northwest, presumably an onshore direction, and channelling is conspicuously uncommon (Coogan et al., 1982). The deposit has been variously attributed to accumulation in a subaerial delta, river system, barrier, bar, lagoon, wind-tidal flat or tidal channel system (Coogan et al., 1982).

Step 1. The symmetrical ripples prove particularly useful in resolving the depositional environment of this unit. The smallest ripples, with a spacing of 1.5 cm, were composed of sand of about 0.01 cm diameter. The λ/D ratio of 150 indicates that the ripples are orbital ripples ($\lambda = 0.65\ d_0$) formed under

an orbital diameter of 2.3 cm. This interpretation is consistent with $\lambda - d_0$ relations predicted by Nielsen's equation for laboratory ripples (Fig.7), which may be more applicable than that for naturally occurring ripples at low values of λ. Equations 19 and 20 indicate maximum wave periods of 1.3 and 1.0 s, respectively, for forming these ripples.

Step 2. The combinations of water depth and wave height whereby a wave with a period of 1.3 s (the more conservative at the indicated values) will generate a near-bottom orbital diameter of 2.3 cm can be estimated using Airy wave theory (eq. 18, this paper). Following the procedure outlined in the previous example, an H—h diagram can be constructed (Fig.14), which indicates that the observed ripples formed in very shallow water (less than 2 m deep).

Step 3. The inference that the ripple-marked sandstone was deposited at water depths smaller than the thickness of the intercalated cross-bed sets imposes special constraints. The nature of the contacts between the two lithologies becomes critical to the interpretation. In every observed case, the planar- or wavy-bedded sandstone sharply overlies the sandstone below and extends gradationally into overlying cross-bedding foresets above. This relation implies that the bedforms that produced the crossbedding migrated over the planar- or wavy-bedded sandstone with the small ripples. The truncated top to the cross-beds indicates that the bedform relief exceeded the thickness of the cross-bedding unit, which in turn generally is greater than the water depth implied by the small symmetric ripples. The implication that the height of the bedforms exceeded (perhaps substantially) the depth of water into which they migrated and the scarcity of current ripples relative to symmetric ripples effectively eliminate a subaqueous origin for the crossbedding. The bedforms are best interpreted as aeolian dunes that migrated over a surface that at least part of the time was the site of interdune ponds.

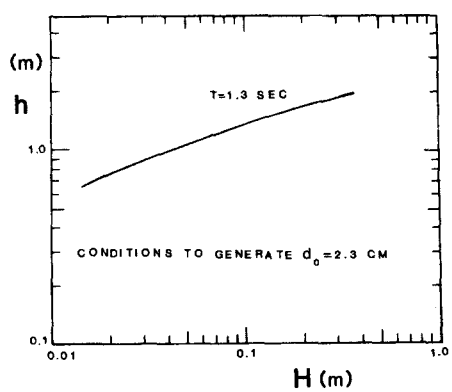

Fig.14. Combinations of water depth and wave height whereby a wave with a period of 1.3 s will generate a near-bottom orbital diameter of 2.3 cm (threshold for forming orbital ripples with a spacing of 1.5 cm in 0.100 mm quartz sand). Wave curve terminated at maximum stable wave height.

Further examination of the deposit supports this interpretation. The wide variability of the trend of the ripple marks (sets on the same bedding surface may diverge by nearly 90°) suggests local winds blowing over very shallow water. Mud cracks on a few of the ripple surfaces are consistent with a pond environment. The crossbedded sand locally shows subtle bedding features (climbing translatent strata, sandflow tongues) attributed to aeolian deposition (Hunter, 1977, 1981).

Other examples. Several recent papers use wave-generated structures to reconstruct paleoenvironments. Allen (1981) uses an approach similar to that analysed in Example 2 to estimate the size and depth of a Devonian lake on southeast Shetland. Clifton (1981) draws heavily on the orientation of wave-formed structures to develop a detailed reconstruction of a Miocene shoreline in the southern Coast Range of California. Papers by Allen and Dupré in this volume provide additional examples.

CONCLUSIONS

Wave-formed sedimentary structures can be a valuable tool for interpreting paleo-environments. A number of caveats should be noted relative to the implementation of these tools:

(1) The results are approximations. The use of wave equations typically gives precise solutions, but the equations themselves are approximations in a real environment. The indicated values should be considered as reasonable estimates only.

(2) Much uncertainty exists regarding the nature of the structures and the hydrodynamic processes involved in their formation. Threshold equations should be extrapolated with care, particularly to the coarser grain sizes. The threshold of movement of large isolated clasts on a bed of smaller material requires further study. The relations between ripple spacing, grain size and orbital diameter need to be defined more closely particularly in terms of the influence of wave period. The basis for asymmetry of wave-formed structures is controversial and awaits further study before being applicable in any hydrodynamic sense.

(3) The interpretation of wave-formed structures is best done in conjunction with other geologic evidence. Inferences of water depth or wave size based on wave-formed features are most credible when supported by other observations.

Much further field observation and experimental study must be done before wave-formed structures reach their full potential for paleoenvironmental interpretation. Presently, they can provide powerful, but often tantalizing, clues regarding ancient environmental conditions.

REFERENCES

Allen, J.R.L., 1970. Physical Processes of Sedimentation. Allen and Unwin, London, 248 pp.

Allen, J.R.L., 1979. A model for the interpretation of wave ripple-marks using their wavelength, textural composition, and shape. J. Geol. Soc. London, 136: 673—682.
Allen, J.R.L., 1980. Sand waves: a model of origin and internal structure. Sediment. Geol., 26: 281—328.
Allen, J.R.L., 1982. Sedimentary Structures — Their Character and Physical Basis, Vol. 1. (Developments in Sedimentology, 30A). Elsevier, Amsterdam, 593 pp.
Allen, P.A., 1981a. Some guidelines in reconstructing ancient sea conditions from wave ripples. Mar. Geol., 43: M59—M67.
Allen, P.A., 1981b. Wave-generated structures in the Devonian lacustrine sediments of south-east Shetland and ancient wave conditions. Sedimentology, 28: 369—379.
Allen, P.A., 1984. Miocene waves and tides from the Swiss Molasse. In: B. Greenwood and R.A. Davis, Jr. (Editors), Hydrodynamics and Sedimentation in Wave-Dominated Coastal Environments. Mar. Geol., 60: 455—473 (this volume).
Bagnold, R.A., 1946. Motion of waves in shallow water. Interaction of waves and sand bottoms. Proc. R. Soc. London, Ser. A, 187: 1—16.
Bagnold, R.A., 1963. Mechanics of marine sedimentation. In: M.N. Hill (Editor), The Sea, Vol. 3. Wiley-Interscience, New York, N.Y., pp. 507—528.
Bagnold, R.A., 1966. An approach to the sediment transport problem from general physics. U.S. Geol. Surv., Prof. Pap., 422-I.
Bascom, W.A., 1980. Waves and Beaches — Revised and updated. Anchor Press/Doubleday, Garden City, N.Y., 366 pp.
Bliven, L., Huang, N.E. and Janowitz, G.S., 1977. An experimental investigation of some combined flow sediment transport phenomena. North Carolina State Univ., Center for Marine and Coastal Studies, Rept. No. 77-3.
Boersma, J.R., 1970. Distinguishing features of wave-ripple cross-stratification and morphology. Thesis, University of Utrecht, Utrecht, 65 pp.
Brebner, A., 1981. Sand bedform lengths under oscillatory motion. Proc. 7th Conf. Coastal Engineering, Sydney, N.S.W., pp.1340—1341.
Bucher, W.H., 1919. On ripples and related sediment surface forms and their paleogeographical interpretations. Am. J. Sci., 47: 149—210, 241—269.
Clifton, H.E., 1976. Wave-generated structures — a conceptual model. In: R.A. Davis and R.L. Ethington (Editors), Beach and Nearshore Processes. Soc. Econ. Paleontol. Mineral., Spec. Publ., 24: 126—148.
Clifton, H.E., 1981. Progradational sequences in Miocene shoreline deposits, southeastern Caliente Range, California. J. Sediment. Petrol., 51: 165—184.
Clifton, H.E., Hunter, R.E. and Phillips, R.L., 1971. Depositional structures and processes in the high-energy nonbarred nearshore. J. Sediment. Petrol., 41: 651—670.
Coogan, A.H., Heimlich, R.A., Malcuit, R.J., Bork, K.B. and Lewis, T.L., 1982. Early Mississippian deltaic sedimentation in central and northeastern Ohio. In: T.G. Roberts (Editor), G.S.A. Cincinnati '81 Field Trip Guidebooks, Vol. 1: Stratigraphy, Sedimentology. Am. Geol. Inst., Falls Church, Va., pp.113—152.
Davidson-Arnott, R.G.D. and Greenwood, B., 1974. Bedforms and structures associated with bar topography in the shallow-water wave environment. J. Sediment. Petrol., 44: 698—704.
Dingler, J.R., 1974. Wave-formed ripples in nearshore sands. Thesis, Univ. Calif. at San Diego, San Diego, Calif., 136 pp.
Dingler, J.R., 1979. The threshold of grain motion under oscillatory flow in a laboratory wave channel. J. Sediment. Petrol., 49: 287—294.
Dingler, J.R. and Clifton, H.E., 1984. Tidal-cycle changes in oscillation ripples on the inner part of an estuarine sand flat. In: B. Greenwood and R.A. Davis, Jr. (Editors), Hydrodynamics and Sedimentation in Wave-Dominated Coastal Environments. Mar. Geol., 60: 219—233 (this volume).
Dingler, J.R. and Inman, D.L., 1977. Wave-formed ripples in nearshore sands. Proc. 15th Conf. on Coastal Engineering, Honolulu, Hawaii, pp.2109—2126.

Dupré, W.R., 1984. Reconstruction of paleo-wave conditions from Pleistocene marine terrace deposits, Monterey Bay, California. In: B. Greenwood and R.A. Davis, Jr. (Editors), Hydrodynamics and Sedimentation in Wave-Dominated Coastal Environments. Mar. Geol., 60: 435—454 (this volume).

Fahnestock, R.K. and Haushild, W.L., 1962. Flume studies of the transport of pebbles and cobbles on a sand bed. Geol. Soc. Am., 73: 1431—1436.

Hallermeier, R.J., 1981. Critical wave conditions for sand motion initiation. Coastal Eng. Tech. Aid No. 81-10, U.S. Army Corps Engineers Coastal Eng. Res. Center, 16 pp.

Harms, J.C., 1969. Hydraulic significance of some sand ripples. Geol. Soc. Am. Bull., 80: 363—396.

Harms, J.C., Southard, J.B. and Walker, R.G., 1982. Structures and sequences in clastic rocks. S.E.P.M. Short Course No. 9, Soc. Econ. Paleontol. Mineral., Tulsa, Okla., 249 pp.

Heezen, B.C. and Hollister, C.D., 1971. The Face of the Deep. Oxford Univ. Press, New York, N.Y., 659 pp.

Hunter, R.E., 1977. Basic types of stratification in small aeolian dunes. Sedimentology, 24: 361—387.

Hunter, R.E., 1981. Stratification styles in eolian sandstones: some Pennsylvanian to Jurassic examples from the western interior, U.S.A. In: F.G. Ethridge and R.M. Flores (Editors), Recent and Ancient Nonmarine Depositional Environments: Models for Exploration. Soc. Econ. Paleontol. Mineral., Spec. Publ., 31: 315—329.

Hunter, R.E. and Clifton, H.E., 1982. Cyclic deposits and hummocky cross-stratification of probable storm origin in Upper Cretaceous area, southwestern Oregon. J. Sediment. Petrol., 52: 127—146.

Inman, D.L., 1957. Wave generated ripples in nearshore sands. Tech. Memo. Beach Erosion. Bd. U.S. Army Corps of Engineers, 100.

Inman, D.L., 1963. Ocean waves and associated currents. In: F.P. Shepard (Editor), Submarine Geology (2nd ed.). Harper and Row, New York, N.Y., pp.49—81.

Inman, D.L. and Bowen, A.J., 1963. Flume experiments on sand transport by waves and currents. Proc. 8th Conf. Coastal Engineering, Berkeley, Calif., pp.137—150.

Iverson, H.W., 1952. Studies of wave transformation in shoaling water, including breaking. Natl. Bur. Stand., Circ., 521: 9—32.

Jonsson, I.G., 1967. Wave boundary layers and friction factors. Proc. 10th Conf. Coastal Engineering, Tokyo, pp.127—148.

Kemp, P.H., 1975. Wave asymmetry in the nearshore zone and breaker area. In: J. Hails and A. Carr (Editors), Nearshore Sediment Dynamics and Sedimentation. Wiley, New York, N.Y., pp.47—65.

Komar, P.D., 1974. Oscillatory ripple marks and the evaluation of ancient wave conditions and environments. J. Sediment. Petrol., 44: 169—180.

Komar, P.D., 1976. Beach Processes and Sedimentation. Prentice-Hall, Englewood Cliffs, N.J., 417 pp.

Komar, P.D. and Miller, M.C., 1973. The threshold of movement under oscillatory water waves. J. Sediment. Petrol., 43: 1101—1110.

Komar, P.D. and Miller, M.C., 1975. The initiation of oscillatory ripple marks and the development of plane-bed at high shear stresses under waves. J. Sediment. Petrol., 45: 697—703.

LeMehaute, B., Divoky, D. and Lin, A., 1969. Shallow water waves: a comparison of theories and experiments. Proc. 11th Conf. Coastal Engineering, London, pp.86—96.

Lofquist, K.E.G., 1978. Sand ripple growth in an oscillatory-flow water tunnel. Tech. Pap. Coastal Eng. Res. Center, U.S. Army Corps Eng., 75-8.

Longuet-Higgins, M.S., 1953. Mass transport in water waves. Philos. Trans. R. Soc. London, Ser. A, 245: 535—581.

Madsen, O.S. and Grant, W.D., 1976. Sediment transport in the coastal environment. Rept. no. 209, Ralph M. Parsons Lab., Mass. Inst. Tech., 105 pp.

Miche, R., 1944. Undulatory movements of the sea in constant and decreasing depth. Ann de Ponts et Chaussées, May—June, July—August, pp.25—78, 131—164, 369—406.

Miller, M.C. and Komar, P.D., 1980a. Oscillation sand ripples generated by laboratory apparatus. J. Sediment. Petrol., 50: 173—182.
Miller, M.C. and Komar, P.D., 1980b. A field investigation of the relationship between oscillation ripples spacing and the near-bottom water orbital motions. J. Sediment. Petrol., 50: 183—191.
Nielsen, P., 1981. Dynamics and geometry of wave-generated ripples. J. Geophys. Res., 86: 6467—6472.
Pepper, J.F., DeWitt, W. and Desmarest, D.F., 1954. Geology of the Bedford shale and Berea sandstone in the Appalachian Basin. U.S. Geol. Surv., Prof. Pap., 259, 106 pp.
Reineck, H.E. and Singh, I.B., 1973. Depositional Sedimentary Environments. Springer, New York, N.Y., 439 pp.
Reineck, H.E. and Wunderlich, F., 1968. Zur Unterscheidung von asymmetrischen Oszillationrippeln und Strömungsrippeln. Senkenbergiana Lethaea, 49: 321—345.
Shields, A., 1936. Anwendung der Ähnlichkeitsmechanik und der Turbulenzforschung auf die Geschiebebewegung. Mitt. Preuss. Versuchsanst. Wasserbau Schiffbau, 26, 20 pp.
Sleath, J.F.A., 1975. A contribution to the study of vortex ripples. J. Hydraul. Res., 13: 315—328.
Sleath, J.F.A., 1976. On rolling-grain ripples. J. Hydraul. Res., 14: 69—81.
Southard, J.B. and Dingler, J.R., 1971. Flume study of ripple propagation behind mounds on flat sand beds. Sedimentology, 16: 251—263.
Stokes, G.G., 1847. On the theory of oscillatory waves. Trans. Cambridge Philos. Soc., 8: 441.
Tanner, W.F., 1967. Ripple mark indices and their uses. Sedimentology, 9: 89—104.
Tanner, W.F., 1971. Numerical estimates of ancient waves, water depth and fetch. Sedimentology, 16: 71—88.
Tietze, K.W., 1978. Zur Geometrie von Wellenrippeln in Sanden unterschiedlicher Korngrösse. Geol. Rundsch., 67: 1016—1033.
U.S. Army Coastal Engineering Research Center, 1973. Shore Protection Manual, 3 vols.
Wells, D.R., 1967. Beach equilibrium and second-order wave theory. J. Geophys. Res., 72: 497—504.
Wiegel, R.L., 1954. Gravity Wave, Tables of Functions. Council on Wave Research, Eng. Found. Univ. California, Berkeley, Calif., 30 pp.
Wiegel, R.L., 1960. A presentation of cnoidal wave theory for practical application. J. Fluid Mech., 7: 273—286.